Journal of Sound and Vibration 326 (2009) 400–420

Contents lists available at ScienceDirect

Journal of Sound and Vibration

journal homepage: www.elsevier.com/locate/jsvi

Optimal semi-active preview control response of a half car vehicle model with magnetorheological damper

R.S. Prabakar, C. Sujatha, S. Narayanan *

Machine Design Section, Department of Mechanical Engineering, Indian Institute of Technology Madras, Chennai 600 036, India

ARTICLE INFO

Article history:
Received 22 June 2008
Received in revised form
14 April 2009
Accepted 23 May 2009
Handling Editor: J. Lam
Available online 23 June 2009

ABSTRACT

The control of the stationary response of a half car vehicle model moving with a constant velocity over a rough road with magnetorheological (MR) dampers is considered. The MR damper is modelled by the modified Bouc–Wen model. The MR damper parameters adopted in the vehicle model correspond to an actual fabricated damper and are determined so that the MR damper model characteristics match with experimental characteristics. The random road excitation is considered as the output of a first-order linear shaping filter to white noise excitation. The control and response statistics of the nonlinear vehicle model with MR damper are obtained using the equivalent linearization method in an iterative manner and the results are verified by Monte-Carlo simulation. The MR damper performance is sought to be improved by suitable choice of input currents to the levels of performance of an active suspension based on H_∞ control without and with preview by a mean square equivalence of respective control forces. The H_∞ optimal control with preview minimizes a performance index which is a weighted sum of vehicle performance measures such as sprung mass acceleration, pitch acceleration, front and rear suspension strokes, road holding and control forces with the weights obtained by solving a multi-objective optimization problem using a non-dominated sorting genetic algorithm II (NSGA II).

1. Introduction

Vehicle suspension systems can be broadly classified as passive, active and semi-active suspension systems. In the passive suspension system, the stiffness and damping parameters are fixed and are effective over a certain range of frequencies. To overcome this problem, the use of active suspension systems which have the capability of adapting to changing road conditions by the use of an actuator have been considered by Karnopp [1]. Hedrick [2], Goodall and Kortum [3] have discussed the theoretical and practical aspects of active suspension design of vehicles. Different optimal control techniques like linear quadratic regulator (LQR) [4], linear quadratic gaussian (LQG) control [5], fuzzy logic [6] and neural network methods have been used in the area of active suspensions.

The performance of the active suspension system can be improved by knowing the future information about the road input which is referred to as 'preview control'. Bender [7] proposed an active suspension system with preview control and used Wiener filter technique to find the optimal control law for a single degree of freedom (dof) vehicle model. The active suspension system with preview control is also applied to a quarter car [8] and half car [9,10] vehicle models. The performance of suspension with preview control is shown to be better than the suspension without preview.

* Corresponding author. Tel.: +91 44 2257 4668; fax: +91 44 2257 4652.
E-mail address: narayans@iitm.ac.in (S. Narayanan).

0022-460X/$ - see front matter © 2009 Elsevier Ltd. All rights reserved.
doi:10.1016/j.jsv.2009.05.032

Increased cost, complexity, need for an external energy source and difficulty in control hardware implementation of active suspension systems led to the development of semi-active suspension systems, which combine the advantages of both passive and active suspension systems. Semi-active suspensions have been considered by a number of authors for vehicular vibration control applications [11–16]. The semi-active suspension system with preview control is also investigated for a quarter car two dof and half car four dof vehicle models by Hac and Youn [17,18], respectively. The results of the semi-active suspension with preview showed improved performance when compared to the semi-active suspension system without preview.

More recently, electrorheological (ER) and magnetorheological (MR) fluids, which can change their viscosity significantly on the application of suitable electrical and magnetic fields, respectively, have also been used in vehicle suspensions as a semi-active suspension system by a number of researchers [19–21]. They considered different control schemes like skyhook, groundhook and a hybrid skyhook and groundhook with minimum or maximum input current to the MR damper depending on the relative velocity between the sprung and unsprung masses. The input current to the MR damper can also be as per different optimal control strategies like LQR, LQG with Kalman filter, neural network and H_∞ controls [22,23]. In the above works, the road excitation is considered as either deterministic or a random process. In the case when the road excitation is treated as a random process it is numerically simulated. The weighting factors used in the controller design are also chosen arbitrarily.

In this paper, the control of the stationary response of a half car vehicle model to random road excitation is considered with optimal semi-active MR dampers. The performance of the MR damper is sought to be matched with the performance of an active suspension using H_∞ control with and without preview in a mean square equivalence sense of the corresponding control forces. Such a formulation is new which enhances the performance of the semi-active suspension almost to the levels of the performance of an active suspension based on a limited state feedback control law using H_∞ control. The MR damper behaviour is modelled by the modified Bouc–Wen model. The MR damper parameters of the model used in the study correspond to an actual damper fabricated in house which uses an indigenously developed MR fluid [24]. An experiment is conducted with the fabricated MR damper by varying the input current from 0 to 1.5 A in intervals of 0.5 A. The model parameters are determined such that the model characteristics fit very closely the experimental hysteretic behaviour of the MR damper. A multi-objective non-dominated sorting genetic algorithm II (NSGA II) technique [25] is used to optimize the modified Bouc–Wen model parameters. It is obtained by minimizing the mean square error between the model and experimental results for the minimum (0 A) and maximum (1.5 A) input currents. The response statistics of the vehicle model with the MR dampers to the random road excitation are obtained using the equivalent linearization technique in an iterative manner, so that stochastic linear optimal control theory can be applied to control the vehicular vibration. As mentioned earlier the intent of the paper is to generate a control force through the nonlinear MR damper which is mean square equivalent to the control force obtained using the H_∞ control so that the semi-active control of the MR damper performs nearly as well as the optimal active control based on limited state feedback using H_∞ control. The results of the equivalent linearization method are verified by Monte-Carlo simulation. Since the aim of the paper is to match the performance of the semi-active MR damper to that of an active suspension, the response of the half car vehicle model using H_∞ control with and without preview is obtained. In the H_∞ control, a performance index which is a weighted sum of the vehicle response measures such as mean square sprung mass acceleration, pitch, front and rear suspension strokes, road holding and control forces, etc. is minimized. The weights corresponding to the vehicle response measures in the performance index are also obtained by solving a multi-objective optimization problem using NSGA II algorithm so that all the response measures are given sufficient importance in the performance index. The matching of the performance of the semi-active MR damper suspension with the activeH_∞ control suspension is realized through a mean square equivalence of the control forces in both the cases and the input currents to the MR damper at different vehicle speeds are correspondingly controlled. Results show that the semi-active MR damper suspension performs significantly better than the passive suspension and approaches the performance of the active suspension with H_∞ control.

2. Random road excitation

The power spectral density (psd) function of road irregularity is assumed to be in the form

$$S_h(\omega) = \frac{\sigma^2}{\pi}\frac{\alpha_r V}{(\omega^2 + (\alpha_r V)^2)} \tag{1}$$

where σ^2 is the variance of the road profile, ω is the circular frequency, V is the vehicle forward velocity and α_r is a coefficient depending on the type of road surface.

In this form, the psd corresponds to the road excitations at the front and rear wheels being the response of a first-order linear filter to white noise and delayed white noise excitations given by

$$\dot{h}_1(t) + \alpha_r V h_1(t) = w(t) \tag{2}$$

$$\dot{h}_2(t) + \alpha_r V h_2(t) = w(t - t_w) \tag{3}$$

where $w(t)$ is a white noise process with covariance function $E[w(t)w^{\mathrm{T}}(\tau)] = Q\delta(t-\tau)$ and Q is the spectral intensity given by $Q = 2\sigma^2\alpha_r V$ and $t_w = (a+b)/V$ is the time delay between the front and rear wheels.

3. Multi-objective optimization

In many practical problems, the design is involved with more than one objective leading to multi-objective optimization problems which are concerned with optimizing more than one objective function. In the present study, a non-dominated sorting genetic algorithm II (NSGA II) is used to solve the multi-objective optimization problem. The algorithm for NSGA II is explained briefly in the sequel. The initial population is created using 0's and 1's for the size of the population. The binary values created are decoded and the objective function is evaluated for the corresponding binary values to get the parent objective function. The fronts are evaluated using the parent objective function values by the concept of non-dominance [25]. The filling of the new population for the next generation starts with the best non-dominated front and continues with second non-dominated front, followed by the third non-dominated front and so on. The crowding distances are calculated for the evaluated fronts by using the concept of crowding distance [25] and are filled along with the new population for the next generation. The best population is found out from the new population for the length of the population size by the concept of crowding tournament selector. Uniform crossover and mutation are performed on the new population to create the child population. Now the parent and child populations are combined and the fronts are found out. This process is repeated for a specified number of generations, for convergence to the optimum.

4. Semi-active MR suspension system

The schematic of the half car model with semi-active suspension provided by MR dampers is shown in Fig. 1(a). The MR damper is modelled by the modified Bouc–Wen hysteretic model shown in Fig. 1(b). The equations of motion of the semi-active MR suspension system with preview are given by

$$M\ddot{y}_c + K_f(y_c + a\theta - y_f) - (U_f)_{\mathrm{MR}} + K_r(y_c - b\theta - y_r) - (U_r)_{\mathrm{MR}} = 0 \tag{4}$$

$$I\ddot{\theta} + K_f(y_c + a\theta - y_f)a - (U_f)_{\mathrm{MR}}a - K_r(y_c - b\theta - y_r)b + (U_r)_{\mathrm{MR}}b = 0 \tag{5}$$

$$m_f\ddot{y}_f + K_{tf}(y_f - h_f) - K_f(y_c + a\theta - y_f) + (U_f)_{\mathrm{MR}} = 0 \tag{6}$$

$$m_r\ddot{y}_r + K_{tr}(y_r - h_r) - K_r(y_c - b\theta - y_r) + (U_r)_{\mathrm{MR}} = 0 \tag{7}$$

where M is the sprung mass of the vehicle body, I is the mass moment of inertia of the vehicle body with respect to centre of gravity (c.g.), m_f and m_r are the unsprung masses, y_c is the absolute displacement of the c.g of the vehicle body (sprung mass), y_f and y_r are the unsprung mass displacements, θ is the pitch angle, K_f and K_r are passive suspension stiffnesses, C_f and C_r are passive suspension damping coefficients, K_{tf} and K_{tr} are the tyre stiffnesses, h_f and h_r are the random road excitations, $(U_f)_{\mathrm{MR}}$ and $(U_r)_{\mathrm{MR}}$ are the control forces generated by the MR dampers. In all these quantities the subscripts 'f' and 'r' refer to the front and rear ends of the vehicle, respectively, and 'MR' refers to the MR damper. a and b are the distances of the front and rear ends from the c.g of the vehicle.

The control forces generated by the front $(U_f)_{\mathrm{MR}}$ and rear $(U_r)_{\mathrm{MR}}$ MR dampers represented in Eqs. (4)–(7) are given by

$$(U_f)_{\mathrm{MR}} = K_{2f}(y_f - y_c - a\theta) + C_{2f}(\dot{y}_{1f} - \dot{y}_c - a\dot{\theta}) \tag{8}$$

$$(U_r)_{\mathrm{MR}} = K_{2r}(y_r - y_c + b\theta) + C_{2r}(\dot{y}_{1r} - \dot{y}_c + b\dot{\theta}) \tag{9}$$

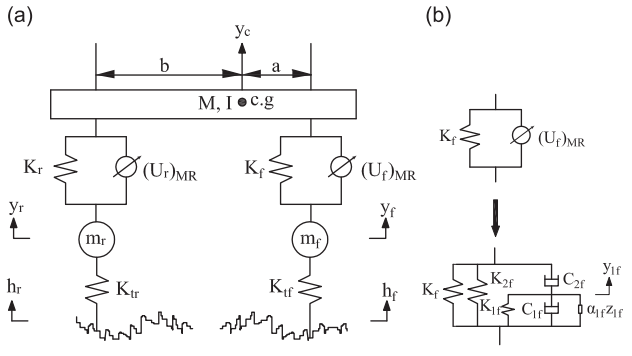

Fig. 1. Semi-active suspension system. (a) Half car with MR damper. (b) The MR damper model.

The velocity components $\dot{y}_{1f}$ and $\dot{y}_{1r}$ in Eqs. (8) and (9), respectively, are given by

$$\dot{y}_{1f} = \frac{1}{C_{1f}+C_{2f}}(K_{1f}(y_f - y_{1f}) + C_{1f}\dot{y}_f + C_{2f}\dot{y}_c + C_{2f}a\dot{\theta} - \alpha_{1f}z_{1f}) \tag{10}$$

$$\dot{y}_{1r} = \frac{1}{C_{1r}+C_{2r}}(K_{1r}(y_r - y_{1r}) + C_{1r}\dot{y}_r + C_{2r}\dot{y}_c - C_{2r}b\dot{\theta} - \alpha_{1r}z_{1r}) \tag{11}$$

y_{1f}, z_{1f}, y_{1r} and z_{1r} correspond to the pre-yielding hysteretic displacements at the front and rear, respectively, of the Bouc–Wen model used to model the behaviour of the damper. The hysteretic displacements z_{1f} and z_{1r} are assumed to be governed by the modified Bouc–Wen model given by [26,27]

$$\dot{z}_{1f} = -\gamma_{1f}|\dot{y}_{1f} - \dot{y}_f|z_{1f}|z_{1f}|^{(n-1)} - \beta_{1f}(\dot{y}_{1f} - \dot{y}_f)|z_{1f}|^n + A_{1f}(\dot{y}_{1f} - \dot{y}_f) \tag{12}$$

$$\dot{z}_{1r} = -\gamma_{1r}|\dot{y}_{1r} - \dot{y}_r|z_{1r}|z_{1r}|^{(n-1)} - \beta_{1r}(\dot{y}_{1r} - \dot{y}_r)|z_{1r}|^n + A_{1r}(\dot{y}_{1r} - \dot{y}_r) \tag{13}$$

where α_{1f}, γ_{1f}, β_{1f} and A_{1f} are the parameters of the Bouc–Wen model, K_{1f} and K_{2f} are the stiffnesses, C_{1f} and C_{2f} are the damping coefficients and y_{1f} and $\dot{y}_{1f}$ are the displacement and velocity of the MR damper model, 'n' is the parameter representing the smoothness of transition from elastic to plastic response. The variables C_{1f}, C_{2f} and α_{1f} are given by a function of input current 'A' as $C_{1f} = C_{1fa} + C_{1fb}A$, $C_{2f} = C_{2fa} + C_{2fb}A$ and $\alpha_{1f} = \alpha_{1fa} + \alpha_{1fb}A$. When the input current A, is zero it corresponds to the passive suspension. The relations referred above are for the front MR damper and similar relations apply to the rear MR damper with the subscript 'f' replaced by 'r'. It is assumed that identical MR dampers are used at the front and the rear, that is, $\alpha_{1f} = \alpha_{1r}$; $\gamma_{1f} = \gamma_{1r}$; $\beta_{1f} = \beta_{1r}$; $A_{1f} = A_{1r}$; $K_{1f} = K_{1r}$; $K_{2f} = K_{2r}$; $C_{1f} = C_{1r}$; $C_{2f} = C_{2r}$.

4.1. Equivalent linearization technique

The response statistics of the vehicle with MR damper are obtained using the equivalent linearization technique [27–30] by which Eqs. (12) and (13) can be approximated by the equivalent linear form

$$\dot{z}_{1f} = -C_{hf}(\dot{y}_{1f} - \dot{y}_f) - K_{hf}z_{1f} \tag{14}$$

$$\dot{z}_{1r} = -C_{hr}(\dot{y}_{1r} - \dot{y}_r) - K_{hr}z_{1r} \tag{15}$$

where C_{hf} and C_{hr} are the equivalent damping coefficients for the front and rear MR dampers, respectively, and K_{hf} and K_{hr} are the equivalent stiffnesses for the front and rear MR dampers, respectively, obtained by minimizing the mean square equation error. These are given by [27,29,30]

$$C_{hf} = \sqrt{\frac{2}{\pi}}\left[\gamma_{1f}\frac{E[(\dot{y}_{1f} - \dot{y}_f)z_{1f}]}{E[(\dot{y}_{1f} - \dot{y}_f)]} + \beta_{1f}E[z_{1f}]\right] - A_{1f} \tag{16}$$

$$K_{hf} = \sqrt{\frac{2}{\pi}}\left[\beta_{1f}\frac{E[(\dot{y}_{1f} - \dot{y}_f)z_{1f}]}{E[z_{1f}]} + \gamma_{1f}E[(\dot{y}_{1f} - \dot{y}_f)]\right] \tag{17}$$

$$C_{hr} = \sqrt{\frac{2}{\pi}}\left[\gamma_{1r}\frac{E[(\dot{y}_{1r} - \dot{y}_r)z_{1r}]}{E[(\dot{y}_{1r} - \dot{y}_r)]} + \beta_{1r}E[z_{1r}]\right] - A_{1r} \tag{18}$$

$$K_{hr} = \sqrt{\frac{2}{\pi}}\left[\beta_{1r}\frac{E[(\dot{y}_{1r} - \dot{y}_r)z_{1r}]}{E[z_{1r}]} + \gamma_{1r}E[(\dot{y}_{1r} - \dot{y}_r)]\right] \tag{19}$$

The equivalent linear parameters C_{hf}, K_{hf}, C_{hr} and K_{hr} given in Eqs. (16)–(19) corresponding to the front and rear MR dampers have to be evaluated iteratively since they are functions of the response statistics. This is done in the following way. Arbitrary small initial values of C_{hf}, K_{hf}, C_{hr} and K_{hr} are assumed and the response statistics evaluated in terms of the zero-lag covariance matrix by solving the matrix Lyapunov equation given in Appendix A. Fresh C_{hf}, K_{hf}, C_{hr} and K_{hr} values are obtained using the response statistics in Eqs. (16)–(19) and again the response statistics are computed. Both the old and new values of C_{hf}, K_{hf}, C_{hr} and K_{hr} are compared for convergence to a specified degree of accuracy. If there is no convergence, then the newly found C_{hf}, K_{hf}, C_{hr} and K_{hr} values are assigned to the old ones and the process is repeated iteratively till the values of C_{hf}, K_{hf}, C_{hr} and K_{hr} converge. It has been found that convergence occurs in less than 10 iterations. The procedure is carried out for the range of vehicle velocities considered to obtain the equivalent linear parameters. It should be mentioned here that the state variables y_{1f}, y_{1r}, z_{1f} and z_{1r} are fictitious variables representing the pre-yielding and hysteretic displacements, respectively, of the modified Bouc–Wen model used to model the behaviour of the MR damper. They are related to the actual state variables y_f, y_r, $\dot{y}_f$, $\dot{y}_r$, $\dot{y}_c$ and $\dot{\theta}$ of the vehicle given by Eqs. (10)–(13). Thus, the states y_{1f}, y_{1r}, z_{1f} and z_{1r} cannot be measured but can be simulated using the state variables y_f, y_r, $\dot{y}_f$, $\dot{y}_r$, $\dot{y}_c$ and $\dot{\theta}$ which can be measured.

4.2. State space representation

The state variables for the half car vehicle model with semi-active suspension system are given by y_c, $\dot{y}_c$, θ, $\dot{\theta}$, y_f, $\dot{y}_f$, y_r, $\dot{y}_r$, y_{1f}, z_{1f}, y_{1r}, z_{1r}, h_f, h_r. Eqs. (4)–(19) representing the vehicle model and Eqs. (2) and (3) representing the road inputs at the front and rear wheels, respectively, can be combined to yield an augmented system of equations expressed as

$$\{\dot{x_a}\} = [F]\{x_a\} + [D_1]\{w(t)\} + [D_2]\{w(t - t_w)\} \tag{20}$$

where $[F]$, $[D_1]$ and $[D_2]$ represent system matrix, excitation matrix corresponding to the front and rear wheel, respectively, and are given in Appendix A. The response statistics of the vehicle can be obtained using the zero-lag covariance matrix by solving the matrix Lyapunov equation also given in Appendix A.

4.3. Optimal MR damper parameters

The MR damper used in the vehicle model with semi-active suspension is an actual MR damper which is fabricated in house. It is a twin tube MR damper whose schematic, the actual assembly and the components are shown in Fig. 2. The fabricated MR damper is tested for sinusoidal excitation with a stroke length of ± 15 mm and a fixed frequency of 1.67 Hz with the MR fluid developed by Reji and Narayana [24]. The test is performed for six cycles for zero current and currents of 0.5, 1.0 and 1.5 A.

The MR damper parameters modelled by the modified Bouc–Wen model are determined to fit the hysteretic behaviour predicted by the model in terms of the force–time, force–displacement and force–velocity characteristics with experimental results obtained doing a dynamic test for different input currents. The parameters are determined by a multi-objective optimization procedure using the NSGA II algorithm in combination with the Pareto optimal scheme minimizing the squared error between the experimental force and the model force generated by the MR damper corresponding to zero input current and the maximum input current of 1.5 A. The details of the experimental investigation

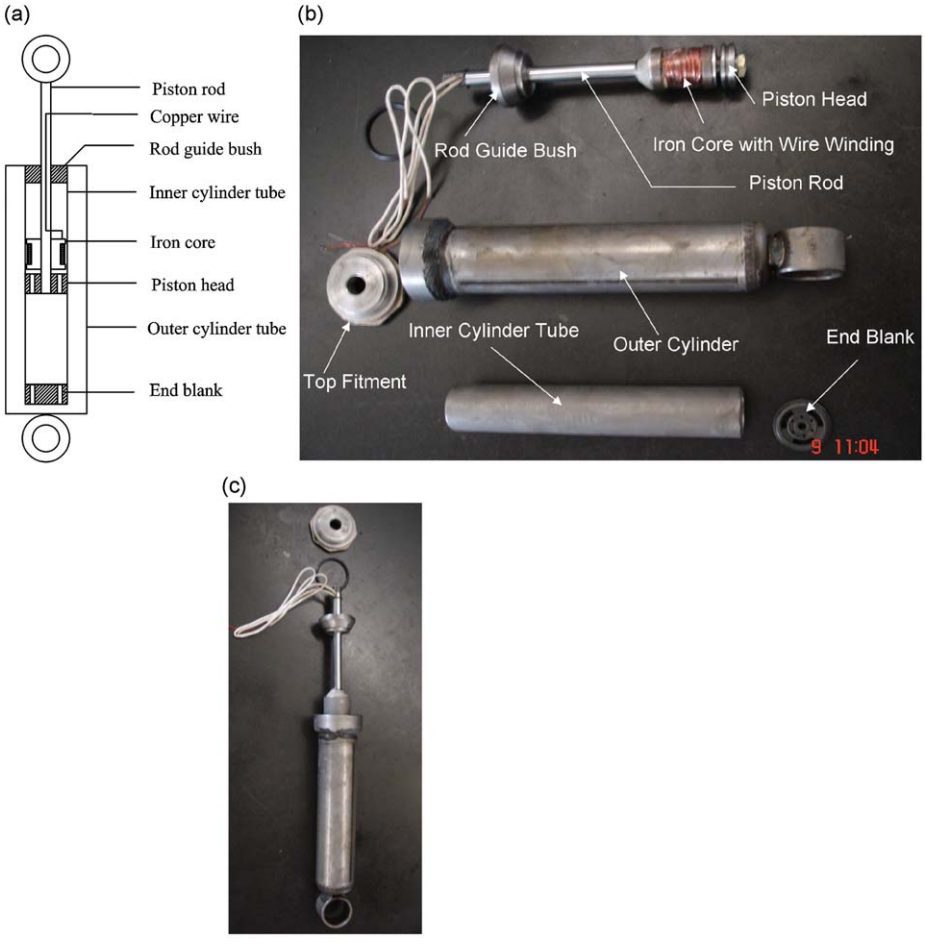

Fig. 2. MR damper details. (a) A schematic diagram of twin tube MR damper. (b) Fabricated MR damper components. (c) MR damper assembly.

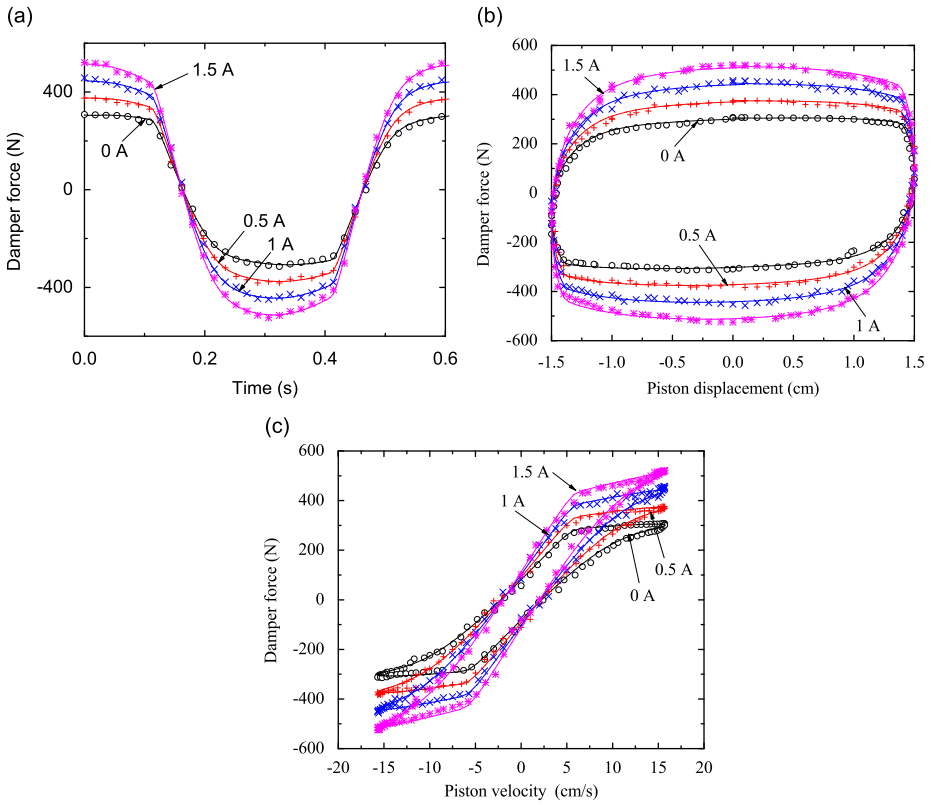

Fig. 3. Experimental dynamic behaviour of fabricated MR damper (experimental ○○○ 0 A, +++ 0.5 A, ××× 1.0 A, ∗∗∗ 1.5 A and theoretical — 0 A, — 0.5 A, — 1.0 A, — 1.5 A). (a) Force versus time plot. (b) Force versus displacement plot. (c) Force versus velocity plot.

are given in Ref. [31]. The agreement between the experimental and theoretical hysteresis curves for these parameters is very good as shown in Fig. 3.

The estimated model parameters of the MR damper are $K_{1f} = 1206.8\,\mathrm{N/m}$; $\alpha_{1fa} = 4179.2\,\mathrm{N/m}$; $K_{2f} = 1017.7\,\mathrm{N/m}$; $\alpha_{1fb} = 1591.7\,\mathrm{N/mA}$; $C_{1fa} = 399.68\,\mathrm{Ns/m}$; $C_{2fa} = 4307.4\,\mathrm{Ns/m}$; $C_{1fb} = 499.06\,\mathrm{Ns/mA}$; $C_{2fb} = 1541.4\,\mathrm{Ns/mA}$; $\beta_{1f} = 8.17\,\mathrm{m^{-1}}$; $\gamma_{1f} = 1183.9\,\mathrm{m^{-1}}$; $A_{1f} = 75.676$.

5. H_∞ active suspension with preview control

The schematic of a half car vehicle model with active and preview control is shown in Fig. 4 and the corresponding equations of motion are given by

$$M\ddot{y}_c + K_f(y_c + a\theta - y_f) + C_f(\dot{y}_c + a\dot{\theta} - \dot{y}_f) - (U_f)_{H_\infty} + K_r(y_c - b\theta - y_r) + C_r(\dot{y}_c - b\dot{\theta} - \dot{y}_r) - (U_r)_{H_\infty} = 0 \tag{21}$$

$$I\ddot{\theta} + K_f(y_c + a\theta - y_f)a + C_f(\dot{y}_c + a\dot{\theta} - \dot{y}_f)a - (U_f)_{H_\infty}a - K_r(y_c - b\theta - y_r)b - C_r(\dot{y}_c - b\dot{\theta} - \dot{y}_r)b + (U_r)_{H_\infty}b = 0 \tag{22}$$

$$m_f\ddot{y}_f + K_{tf}(y_f - h_f) - K_f(y_c + a\theta - y_f) - C_f(\dot{y}_c + a\dot{\theta} - \dot{y}_f) + (U_f)_{H_\infty} = 0 \tag{23}$$

$$m_r\ddot{y}_r + K_{tr}(y_r - h_r) - K_r(y_c - b\theta - y_r) - C_r(\dot{y}_c - b\dot{\theta} - \dot{y}_r) + (U_r)_{H_\infty} = 0 \tag{24}$$

where C_f and C_r are the suspension damping coefficients, P_D is the preview distance, $(U_f)_{H_\infty}$ and $(U_r)_{H_\infty}$ are the control forces which are assumed to be generated as per H_∞ control law and the details of which are given in Section 5.2.

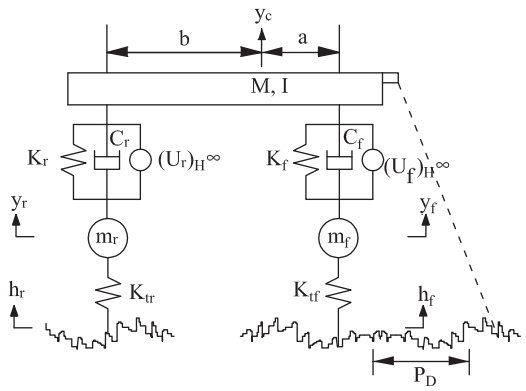

Fig. 4. Active suspension system with preview.

5.1. State space representation

The state variable vector for the half car vehicle model with active suspension system including the road inputs as augmented state variables are given by $\{x_a\}^T = [y_c, \dot{y}_c, \theta, \dot{\theta}, y_f, \dot{y}_f, y_r, \dot{y}_r, h_f, h_r]$. Eqs. (21)–(24) representing the vehicle model and Eqs. (2) and (3) representing the road inputs at the front and rear wheels, respectively, can now be combined to yield an augmented system of equations

$$\{\dot{x_a}\} = [F]\{x_a\} + [G]\{U\} + [D_1]\{w(t)\} + [D_2]\{w(t - t_w)\} \tag{25}$$

where $[F]$, $[G]$, $[D_1]$ and $[D_2]$ represent system matrix, control matrix, excitation matrix corresponding to the front and rear wheel, respectively, and are shown in Appendix A.

5.2. H_∞ control with limited state feedback

The H_∞ optimal control law with limited state feedback is obtained by minimizing a performance index which is the weighted sum of the mean square values of the sprung mass vertical acceleration, pitch acceleration, front and rear suspension strokes, road holding and control forces. The performance index can be expressed as

$$J = \lim_{T\to\infty} \frac{1}{2T} \int_0^T (\rho_1 J_1 + \rho_2 J_2 + \rho_3 J_3 + \rho_4 J_4 + \rho_5 J_5 + \rho_6 J_6 + \rho_7 J_7 + \rho_8 J_8)\,dt \tag{26}$$

where T is the control time period, $J_1 = E[\ddot{y}_c^2]$, $J_2 = E[\ddot{\theta}^2]$, $J_3 = E[(y_c + a\theta - y_f)^2]$, $J_4 = E[(y_c - b\theta - y_r)^2]$, $J_5 = E[(y_1 - h_1)^2]$, $J_6 = E[(y_2 - h_2)^2]$, $J_7 = E[(U_f)^2_{H_\infty}]$ and $J_8 = E[(U_r)^2_{H_\infty}]$, ρ_i, $i = 1, \ldots, 8$ are the weighting constants which decide the performance of the active suspension system with respect to ride comfort, suspension stroke, road holding and control force, respectively, and $E[\cdot]$ represents the expectation operator. The weighting parameters ρ_1, $\rho_2 \cdot \rho_8$ are normally chosen depending on the designer's relative importance given to the various performance measures. In this paper, a new method using a multi-objective optimization scheme is adopted to obtain an optimal choice of the parameters so that all the performance measures are weighted with sufficient importance.

Eq. (26) can be represented in the form [32]

$$J = \lim_{T\to\infty} \frac{1}{2T} \int_0^T E[\{x_a\}^T[A]\{x_a\} + 2\{x_a\}^T[N]\{U\} + \{U\}^T[B]\{U\} - \Gamma^2\{w\}^T\{w\}]\,dt \tag{27}$$

where Γ is the performance bound, $[A] = [C_{yu}]^T[C_{yu}]$ is a symmetric positive semi-definite matrix, $[B] = [D_{yu}]^T[D_{yu}]$ is a positive definite matrix and $[N] = [C_{yu}]^T[D_{yu}]$. The matrices $[C_{yu}]$ and $[D_{yu}]$ are given in Appendix B.

The states are assumed to be measured in the presence of zero mean Gaussian white noise and the measurement vector $\{\psi\}$ is given by

$$\{\psi\} = [C_m]\{x_a\} + \{\zeta\} \tag{28}$$

where $[C_m]$ is the state to measurement transition matrix and $\{\zeta\}$ is the measurement noise which is independent of the state vector $\{x_a\}$ with covariance $E[\{\zeta(t_1)\}\{\zeta(t_2)\}^T] = [R]\delta(t_2 - t_1)$. $[R]$ is a positive definite matrix representing measurement errors.

It is assumed that the relative displacement and velocity between the sprung and unsprung masses are available for estimation by the H_∞ filter. The control vector of the system $\{U\}$ given in Eq. (25) minimizing the performance index given in Eq. (27) along with the preview in the case of limited state feedback is given by [32]

$$\{U\} = -\{C_a\}\{\hat{x}_a\} + \{C_b\}\{r(t)\} \tag{29}$$

where $\{\hat{x}_a(t)\}$ is the optimal estimate vector of the system states, $r(t)$ is a vector containing the preview term which includes look ahead and wheel base preview and are given by

$$r(t) = \int_0^{t_p} \exp[([F] - [G][C_a])^{\mathrm{T}}\sigma][S][D_1]w(t+\sigma)\,\mathrm{d}\sigma + \int_0^{t_p+t_w} \exp[([F] - [G][C_a])^{\mathrm{T}}\sigma][S][D_2]w(t+\sigma-t_w)\,\mathrm{d}\sigma \tag{30}$$

where t_p is the preview time and $\{C_a\}$ and $\{C_b\}$ are the feedback and feed forward control gain vectors given by

$$\{C_a\} = [B]^{-1}([N]^{\mathrm{T}} + [G]^{\mathrm{T}}[S]); \{C_b\} = -[B]^{-1}[N]^{\mathrm{T}} \tag{31}$$

and $[S]$ is the steady-state solution of matrix Riccati equation given by

$$\begin{aligned}&[S]([F] - [G][B]^{-1}[N]^{\mathrm{T}}) + ([F] - [G][B]^{-1}[N]^{\mathrm{T}})^{\mathrm{T}}[S] - [S]([G][B]^{-1}[G]^{\mathrm{T}}\\ &\quad - \Gamma^{-2}[D][D]^{\mathrm{T}})[S] + ([A] - [N][B]^{-1}[N]^{\mathrm{T}}) = 0\end{aligned} \tag{32}$$

The performance bound Γ is evaluated using the bisection algorithm [33]. The optimal estimate of the state vector of the system states $\{\hat{x}_a\}$ is governed by

$$\{\dot{\hat{x}}_a\} = [F]\{\hat{x}_a\} + [G]\{U\} + \{L\}(\{m\} - [C_m]\{\hat{x}_a\}) \tag{33}$$

where $\{L\}$ is the H_∞ filter gain vector given by

$$\{L\} = [P][C_m]^{\mathrm{T}}[R]^{-1} \tag{34}$$

In Eq. (34), $[P]$ is the covariance matrix of the estimation error $e = \{x_a\} - \{\hat{x}_a\}$, i.e., $[P] = E[(\{x_a\} - \{\hat{x}_a\})(\{x_a\} - \{\hat{x}_a\})^{\mathrm{T}}]$. It is the solution of the matrix Riccati equation given by

$$\begin{aligned}&[F][P] + [P][F]^{\mathrm{T}} - [P]([C_m]^{\mathrm{T}}[R]^{-1}[C_m] - \Gamma^{-2}[C_{yu}]^{\mathrm{T}}[C_{yu}])[P] + [D_1][Q][D_1]^{\mathrm{T}}\\ &\quad + [D_2][Q][D_2]^{\mathrm{T}} + \phi(t,t-t_w)[D_1][Q][D_2]^{\mathrm{T}} + [D_2][Q][D_1]^{\mathrm{T}}\phi(t,t-t_w)^{\mathrm{T}}\\ &\quad \times P_1 D_1^{\mathrm{T}} + D_1 P_1^{\mathrm{T}} + P_2 D_2^{\mathrm{T}} + D_2 P_2^{\mathrm{T}} = 0\end{aligned} \tag{35}$$

where ϕ is the state transition matrix and is given by

$$\phi(t_1,t_2) = \exp[[F] - [G]\{C_a\}(t_1 - t_2)] \tag{36}$$

The terms P_1 and P_2 are given in Appendix C.

The mean square values of the states are given by

$$[Z] = [\hat{Z}] + [P] \tag{37}$$

where $[\hat{Z}]$ is the state estimate matrix which is governed by the Lyapunov equation

$$([F] - [G][C])[\hat{Z}] + [\hat{Z}]([F] - [G][C])^{\mathrm{T}} + [L][R][L]^{\mathrm{T}} = 0 \tag{38}$$

5.3. Optimal choice of weighting factors

The weighting parameters $\rho_1, \rho_2, \ldots, \rho_8$ in the performance index for H_∞ control are chosen using a multi-objective constrained optimization procedure. The weighting parameters corresponding to the sprung mass acceleration, pitch acceleration and the value of R are fixed at constant values of $\rho_1 = 1$, $\rho_2 = 1$ and $R = 10^{-3}$ and the weighting parameters $\rho_3 - \rho_8$ are obtained optimally with a constraint on the H_∞ control force to lie between the control force of the MR damper for zero input current and maximum input current of 1.5 A, respectively. The choice of the weighting factors in this way is to assure a balance of good performance with respect to all performance measures namely sprung mass acceleration, pitch acceleration, front and rear suspension strokes, road holdings with reasonable control effort and at different vehicle speeds and the H_∞ control effort will be possibly matched by the control effort of the MR damper.

The constrained optimization problem is to obtain an optimal combination of $\rho_3 - \rho_8$ minimizing three objectives namely sprung mass acceleration (J_1), combination of front and rear suspension strokes ($J_3 + J_4$) and combination of front and rear road holding ($J_5 + J_6$) with the following constraint:

$$E[(U_f)^2_{\mathrm{MR}_{0A}}] \leqslant E[(CF_f)^2_{H_\infty}] \leqslant E[(U_f)^2_{\mathrm{MR}_{1.5A}}] \tag{39}$$

$$E[(U_r)^2_{\mathrm{MR}_{0A}}] \leqslant E[(CF_r)^2_{H_\infty}] \leqslant E[(U_r)^2_{\mathrm{MR}_{1.5A}}] \tag{40}$$

where $(CF_f)_{H_\infty}$ represents the combined force from the active system using the H_∞ control and the damping force corresponding to the linear passive system given in Eqs. (21)–(24) at the front wheel namely $(CF_f)_{H_\infty} = (U_f)_{H_\infty} + C_f(\dot{y}_c + a\dot{\theta} - \dot{y}_f)$. Similarly, the combined control force from the H_∞ control and the damping corresponding to the linear passive system for the rear wheel is given as $(CF_r)_{H_\infty} = (U_r)_{H_\infty} + C_r(\dot{y}_c - b\dot{\theta} - \dot{y}_r)$. The subscript H_∞ refers to the active control scheme. $(U_f)_{\mathrm{MR}_{0A}}$, $(U_r)_{\mathrm{MR}_{0A}}$, $(U_f)_{\mathrm{MR}_{1.5A}}$ and $(U_r)_{\mathrm{MR}_{1.5A}}$ are the forces generated by the MR damper as given in

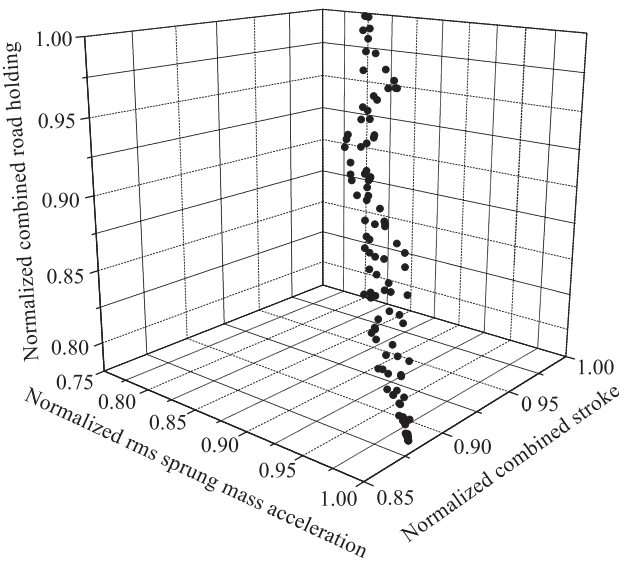

Fig. 5. Pareto optimal solution.

Eqs. (8) and (9). The subscripts MR_{0A} and $MR_{1.5A}$ refer tothe MR damper input currents of 0 and 1.5 A, respectively. The front and rear MR damper forces represented in the equations are evaluated using Eqs. (10)–(19). The combined forces from the active system using the H_∞ control and the damping force corresponding to the linear passive system at the front and rear are restricted to lie between the minimum and maximum forces generated by the MR damper as per Eqs. (39) and (40). These constraints on the control forces are imposed since the motive is to obtain a performance using semi-active control with MR dampers to match the performance of the active H_∞ control corresponding to the linear system with passive spring and damping elements through a mean square equivalence of the respective control forces.

The multi-objective optimization problem is solved by the NSGA II algorithm with the following parameters, population size = 100, probability of cross over = 0.9, probability of mutation = 0.01, number of generations = 150 in combination with the Pareto optimal scheme. The mean square control forces corresponding to the MR damper in the constraint inequalities (39) and (40) are evaluated using the equivalent linear model presented in Section 4. The front and rear equivalent damping coefficients C_{hf}, C_{hr} and the front and rear equivalent stiffnesses K_{hf}, K_{hr} are obtained as per Eqs. (16)–(19) iteratively as they depend on the response statistics.

The normalized Pareto optimal front corresponding to the combination of optimal solutions minimizing the sprung mass acceleration, front and rear suspension strokes and road holdings, respectively, is shown in Fig. 5. The optimized values of the weighting functions are $\rho_3 = 31.623$; $\rho_4 = 98.958$; $\rho_5 = 5551.6$; $\rho_6 = 1224.1$; $\rho_7 = 1.64 \times 10^{-6}$; $\rho_8 = 2.11 \times 10^{-8}$. These weighting constants are good for a range of velocities (0–24 m/s). Once the optimal weighting constants are determined the performance of the vehicle with semi-active suspension using MR damper is sought to be matched with the performance of the H_∞ controller with the limited state feedback by a suitable choice of input currents to the MR damper for different velocities. This is done by equating the mean square control force of the H_∞ controller to that of the MR damper.

6. System response in frequency domain

The response of the system can also be obtained in the frequency domain for passive, semi-active and active suspensions with and without preview. For the passive and semi-active suspensions from Eq. (20) we get the psd of the response as

$$S_{x_a x_a}(\omega) = H(\omega)(D_1 S_{ww} D_1^* + D_2 S_{ww} D_2^* + \phi D_1 S_{ww} D_2^* + D_2 S_{ww} D_1^* \phi^{\mathrm{T}}) H^*(\omega) \tag{41}$$

where $S_{ww} = 2\sigma^2 \alpha V/\pi$, $H(\omega) = 1/(\mathrm{j}\omega I_d - F)$ is the corresponding complex frequency response matrix, with I_d being the identity matrix and $j = \sqrt{-1}$, ϕ is the state transition matrix and F is the system matrix. The asterisk represents both complex conjugation and transpose of the corresponding matrices. Similarly, for the active suspension with preview from Eqs. (25), (29)–(38), the psd of the response $S_{x_a x_a}(\omega)$ is given by [34]

$$S_{x_a x_a}(\omega) = H(\omega) D_R(\omega) S_{ww} D_R^*(\omega) H^*(\omega) \tag{42}$$

with $H(\omega)$ in this case given by $H(\omega) = 1/(\mathrm{j}\omega I_d - (F - GC_a))$ and $D_R(\omega)$ is given by

$$D_R(\omega) = \left(GC_b \left(\int_0^{t_p} \exp[([F] - [G][C_a])^{\mathrm{T}}\sigma][S][D_1] \exp(\mathrm{j}\omega\sigma)\,\mathrm{d}\sigma + \int_0^{t_p+t_w} \exp[([F] - [G][C_a])^{\mathrm{T}}\sigma][S][D_2] \exp(\mathrm{j}\omega(\sigma - t_w))\,\mathrm{d}\sigma \right) + D_1 + D_2 \right) w(\mathrm{j}\omega)$$

The psd of the response for the active suspension without preview can be obtained by setting the preview time $t_p = 0$.

7. Monte-Carlo simulation technique

To check the accuracy of the equivalent linearization technique, Monte-Carlo simulation technique is adopted [35]. The white noise with one sided psd $S_0(\omega) = \sigma^2 \alpha_r V/\pi$ is simulated by the series

$$w(t) = \sqrt{2} \sum_{k=1}^{N} [S_0(\omega_k)\Delta\omega]^{1/2} \cos(\omega'_k t + \phi_k) \tag{43}$$

with $\omega_k = \omega_l + (k - \frac{1}{2})\Delta\omega$, $k = 1, 2, 3, \ldots, N$, $\Delta\omega = (\omega_u - \omega_l)/N$, ω_l and ω_u are the lower and upper cutoff frequencies, respectively, N is the number of intervals, $\omega'_k = \omega_k + \delta\omega$ in which $\delta\omega$ is a small random frequency uniformly distributed between $-\Delta\omega'/2$ and $\Delta\omega'/2$ with $\Delta\omega' \gg \Delta\omega$, ϕ_k is the independent random phase uniformly distributed between 0 and 2π.

The parameters used for generating the time histories are $N = 1000$, $\omega_l = 0\,\mathrm{rad/s}$, $\omega_u = 2 \times \pi \times 100\,\mathrm{rad/s}$ and $\Delta\omega' = 0.05\Delta\omega$. The psd of the road surface is obtained using the MATLAB command 'psd' from the time histories for the road input generated using Eq. (43) and is compared with the targeted frequency obtained from Eq. (1). The comparison is shown in Fig. 6 which shows good agreement between the targeted and simulated psds.

8. Results and discussion

The results of the stationary response of a four dof vehicle model using passive, semi-active MR damper control and H_∞ control to random road excitation are presented in this section. The half car vehicle model with the following parameters is considered as an example. $M = 1200$, $m_f = 75$, $m_r = 80\,\mathrm{kg}$, $I = 1800\,\mathrm{kg\,m^2}$, $K_f = 30\,\mathrm{kN/m}$, $K_r = 30\,\mathrm{kN/m}$, $C_f = 400\,\mathrm{Ns/m}$, $C_r = 450\,\mathrm{Ns/m}$, $K_{tf} = 300\,\mathrm{kN/m}$, $K_{tr} = 300\,\mathrm{kN/m}$, $a = 1.011\,\mathrm{m}$, $b = 1.803\,\mathrm{m}$ and the road parameters used in the analysis are $\alpha_r = 0.45\,\mathrm{rad/m}$ and $\sigma^2 = 3 \times 10^{-4}\,\mathrm{m^2}$.

The rms sprung mass acceleration, rms pitch acceleration, rms front and rear suspension strokes, road holdings, control forces, input currents and overall performances are computed for the vehicle with the (a) passive suspension (MR damper with 0 A), (b) optimal active suspension system based on H_∞ control without preview, (c) optimal active suspension system based on H_∞ control with preview, (d) semi-active suspension with MR damper and mean square equivalent control force of H_∞ control without preview, (e) semi-active suspension with MR damper and mean square equivalent control force of H_∞ control with preview. The responses corresponding to the optimal active suspension system with H_∞ control and the semi-active suspension with MR damper and with mean square equivalent control force of H_∞ control without preview are obtained by setting the preview distance $P_D = 0$.

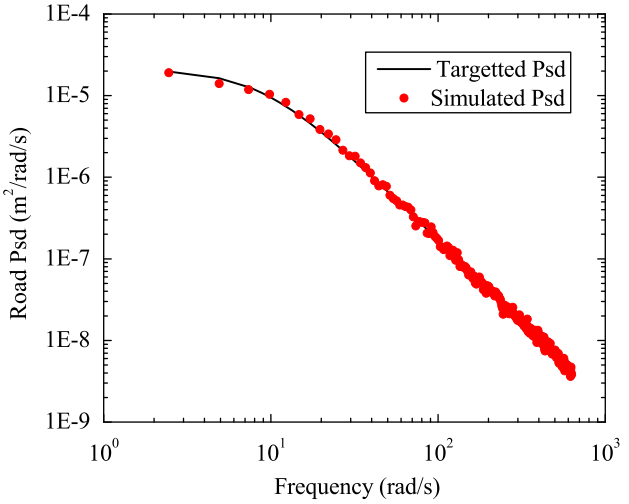

Fig. 6. Psd of road profile.

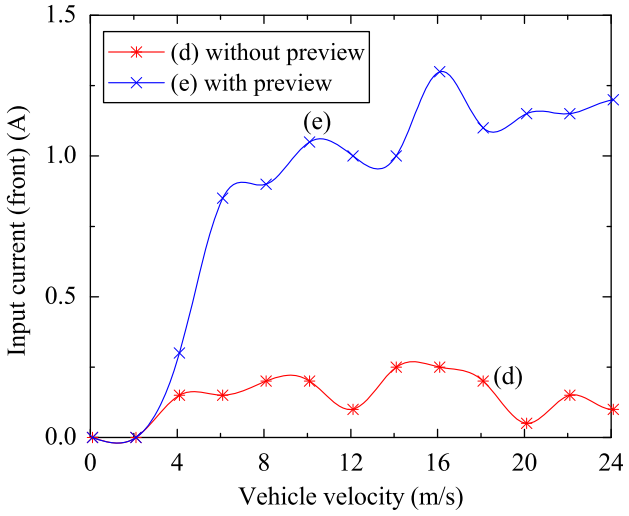

Fig. 7. Input current to front MR damper corresponding to mean square equivalence of control force with H_∞ control force.

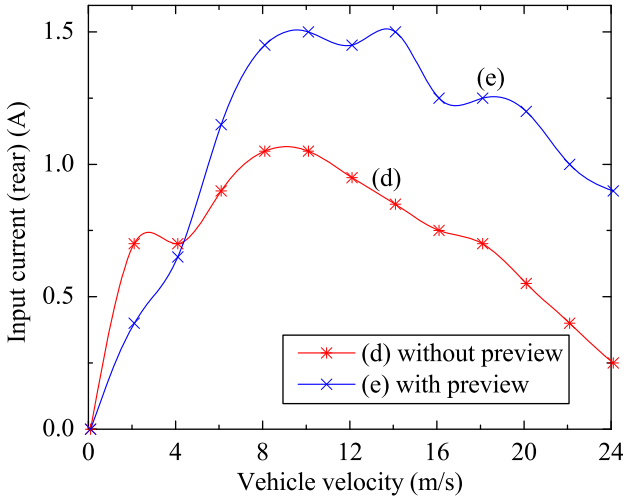

Fig. 8. Input current to rear MR damper corresponding to mean square equivalence of control force with H_∞ control force.

The input currents to the front and rear MR dampers corresponding to mean square equivalence of the control forces with H_∞ control forces with and without preview are shown in Figs. 7 and 8, respectively. The input currents to the front and rear semi-active MR damper without preview (d) and with preview (e) are obtained by matching the corresponding control forces with that of the H_∞ controller without preview (b) and with preview (c), respectively, in a mean square equivalence sense. For this road input and for a given velocity of traverse of the vehicle, the MR damper input currents (front and rear) are constants. It is seen that the input current requirement for matching the H_∞ control force with preview is more than that without preview. This is so because the control force required for the active suspension system with preview is more than the control force without preview.

The rms control forces generated by the MR damper for these input currents and the H_∞ control forces without and with preview are shown in Figs. 9 and 10, respectively, showing very good agreement between them. The control force corresponding to the passive suspension system (MR damper with 0 A) is also shown in the figures. The rms control forces for the MR damper with zero input current (passive) and with the mean square equivalent control forces without and with preview are also obtained by Monte-Carlo simulation [35]. The random road profiles are generated compatible with the power spectral density given in Eq. (1) using a sum of cosine functions with random frequency and phase and the nonlinear equations of motion are numerically integrated to get the mean square control forces. These are shown in Figs. 9 and 10 by the symbols •, ○, ⋆. It is observed that the results of the equivalent linearization method agree well with the simulation results validating the efficiency of the equivalent linearization method.

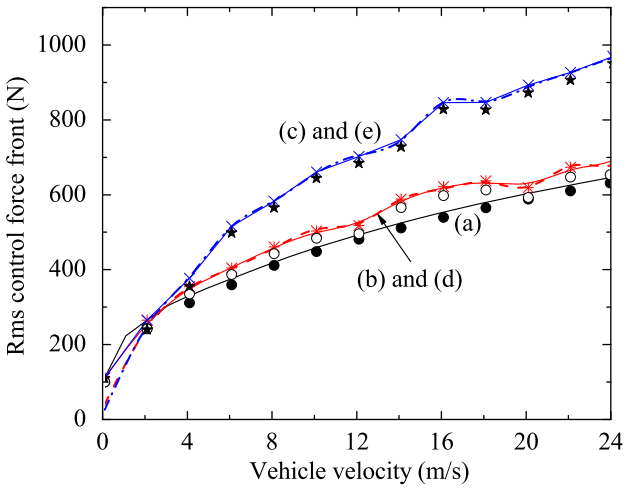

Fig. 9. Rms control force at front —- (a) passive; - - - (b) H_∞ without preview; – · – · – (c) H_∞ without preview; –×– (d) MR damper with mean square equivalent H_∞ control force without preview; –✳– (e) MR damper with mean square equivalent H_∞ control force with preview; •, ○ and ⋆ Monte-Carlo simulation results corresponding to (a), (d) and (e).

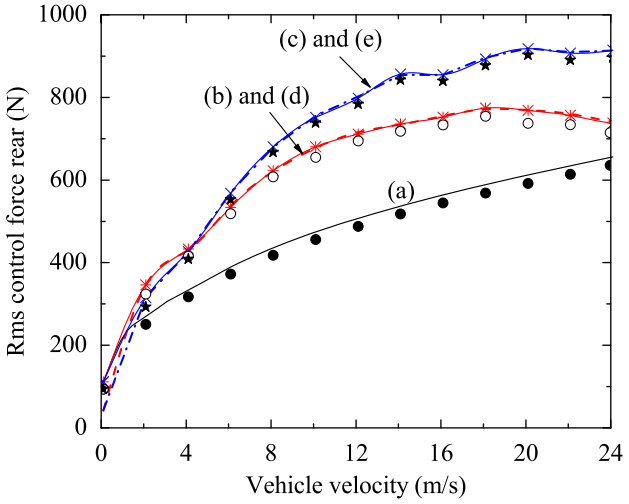

Fig. 10. Rms control force at rear (legends as in Fig. 9).

The overall performance as per Eq. (26) corresponding to the passive suspension, H_∞ control without and with preview and the MR damper suspension corresponding to the input currents of Figs. 7 and 8 are shown in Fig. 11. It is seen from the figure that the overall performances with semi-active MR damper suspension with mean square equivalence of H_∞ control force without and with preview are much better than the performance with the passive suspension system. However, the performance with the MR damper does not measure up to the performance of the H_∞ control especially at higher velocities. The performance of the MR damper with mean square control force equivalent to the H_∞ control force with preview is better than the performance of the MR damper with the mean square control force equivalent to the H_∞ control force without preview. As seen from the figures the performance with H_∞ optimal control with preview is much better than the performance with H_∞ control without preview. These performances are better than the corresponding performances of the MR damper.

From Fig. 12 it is observed that the MR damper with mean square equivalent H_∞ control force without and with preview performs better than the passive suspension with respect to the sprung mass acceleration. But the performance does not measure up to the corresponding performance of the active suspension with H_∞ control without and with preview, respectively. It is also seen that the preview information improves the performance of the suspension without preview both with H_∞ control and with MR damper. The Monte-Carlo simulation results which are also shown in the figures agree well with the equivalent linearization results, validating the equivalent linearization method.

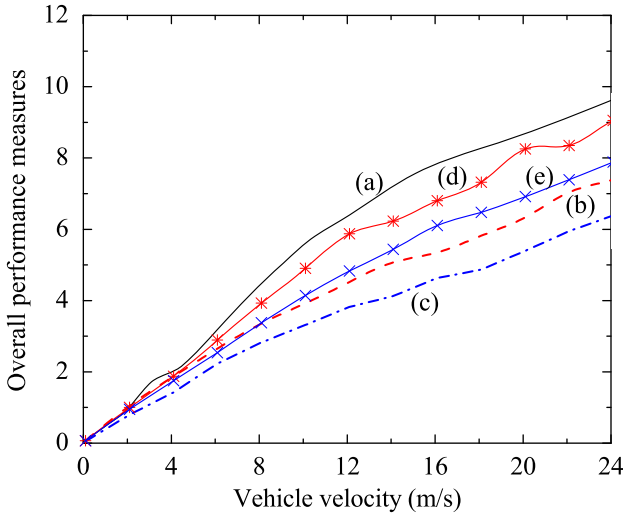

Fig. 11. Overall performance of the vehicle for different control schemes (legends as in Fig. 9).

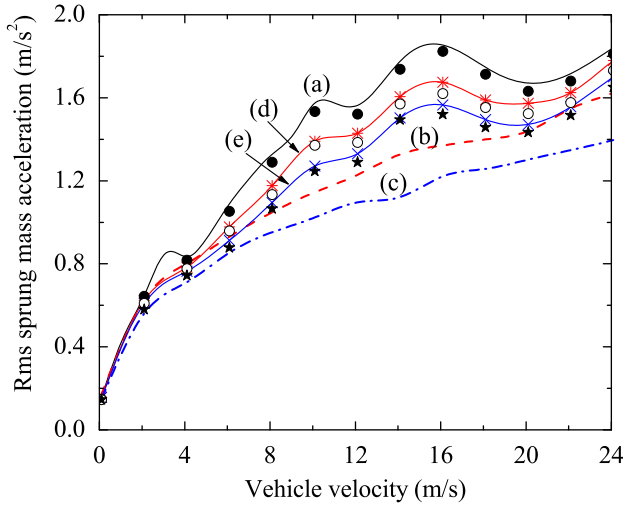

Fig. 12. Rms sprung mass acceleration response (legends as in Fig. 9).

In Fig. 13, the rms value of the pitch acceleration is plotted for different vehicle velocities. Similar trends as for the sprung mass acceleration response are observed in this case also. The performance of the MR damper with mean square equivalent H_∞ control force with preview is better than corresponding to the mean square equivalent H_∞ control force without preview. The H_∞ controls without and with preview perform better than the corresponding MR damper suspension. The performance of the MR damper is much better than the performance of the passive suspension. Again Monte-Carlo simulation results validate the equivalent linearization results.

The rms suspension strokes at the front for all the cases of control are shown in Fig. 14. In this case also the suspension with mean square control force equivalent to the H_∞ control force without and with preview perform better than the passive suspension. But the performances do not measure up to the performances of the corresponding active suspension with H_∞ control without and with preview. The equivalent linearization results are in agreement with Monte-Carlo simulation results.

The rear rms suspension stroke responses are shown in Fig. 15. In this case, the MR damper suspension performances with mean square equivalent H_∞ control force without and with preview are much better than the corresponding H_∞ control performance and also much better than the passive suspension performance. In fact the H_∞ control force

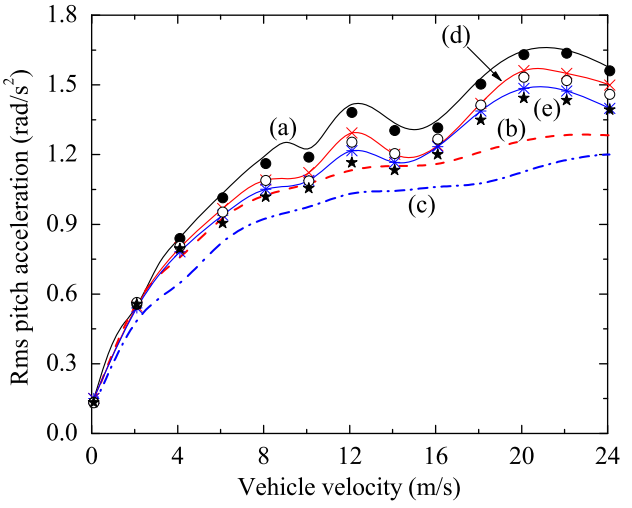

Fig. 13. Rms pitch acceleration response (legends as in Fig. 9).

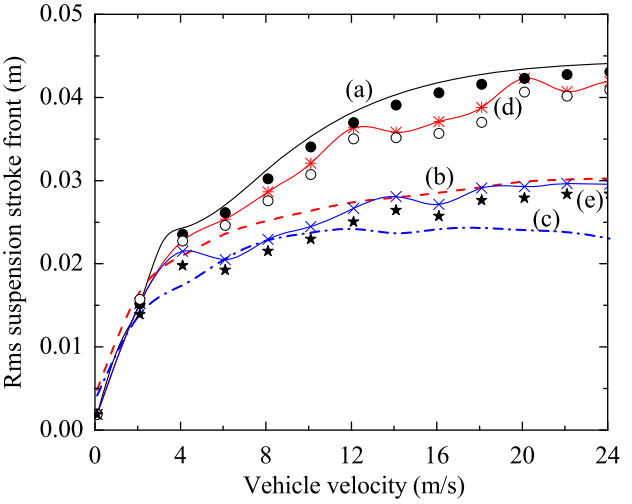

Fig. 14. Rms suspension stroke response at front (legends as in Fig. 9).

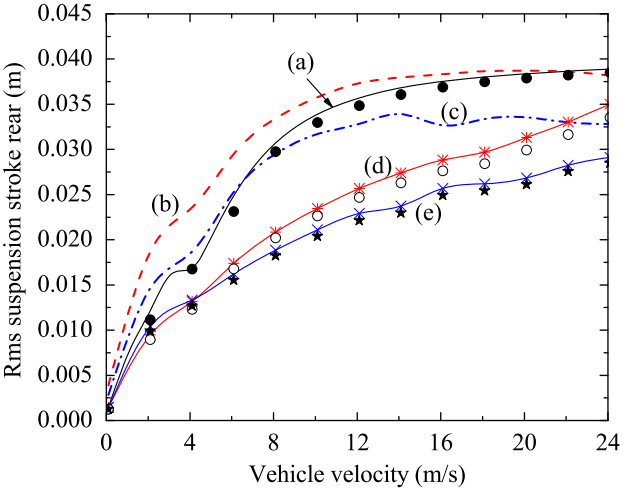

Fig. 15. Rms suspension stroke response at rear (legends as in Fig. 9).

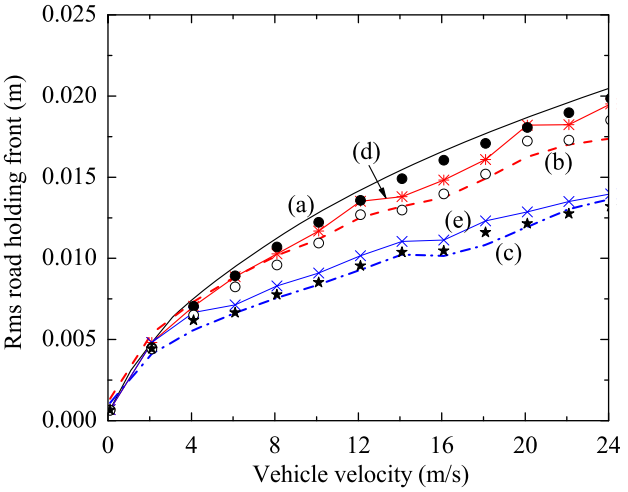

Fig. 16. Rms road holding response at front (legends as in Fig. 9).

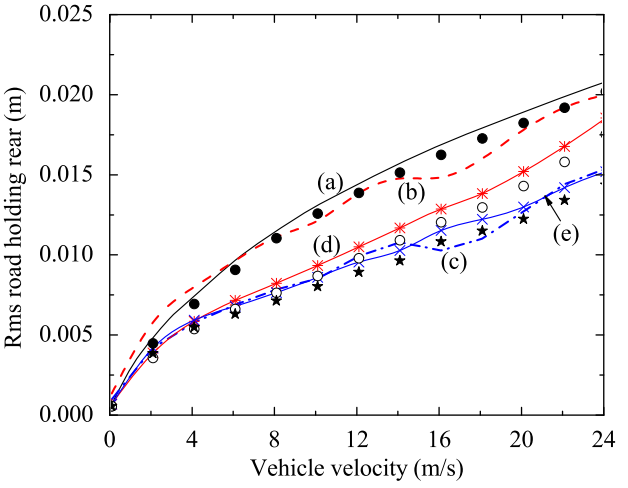

Fig. 17. Rms road holding response at rear (legends as in Fig. 9).

performance without preview is worse than that of the passive suspension. This may be due to the fact that the optimal weighting factors in the performance index determined are based on the preview information. Moreover, the performance index with respect to the suspension strokes is a combination of both the front and rear suspension strokes and does not consider them individually. Because of this it may be possible that the rear suspension stroke is not properly weighted in the performance index and hence its performance is degraded in the control scheme. This deterioration in performance is alleviated slightly with the preview information. Once again the results for the MR damper suspension are verified with Monte-Carlo simulation results.

The rms road holding responses at front and rear are plotted for all the control schemes as a function of velocity in Figs. 16 and 17, respectively. In these cases also the performances of the MR damper with mean square equivalent H_∞ control force with preview are better than the MR damper performances with mean square equivalent H_∞ control force without preview. In the case of the front road holding response the MR damper performances with mean square equivalent H_∞ control force without and with preview are almost as good as the performance of the H_∞ control without and with preview. In the case of the rear road holding response the MR damper with mean square equivalent H_∞ control force without preview performs even better than the corresponding H_∞ control. The MR damper with mean square equivalent H_∞ control force with preview performs as well as the corresponding H_∞ control. All these responses are better than the response of the passive suspension system. But in the case of the rear road holding the H_∞ control without preview performs only marginally better than the passive suspension. This may be also due to the fact that as in the case of

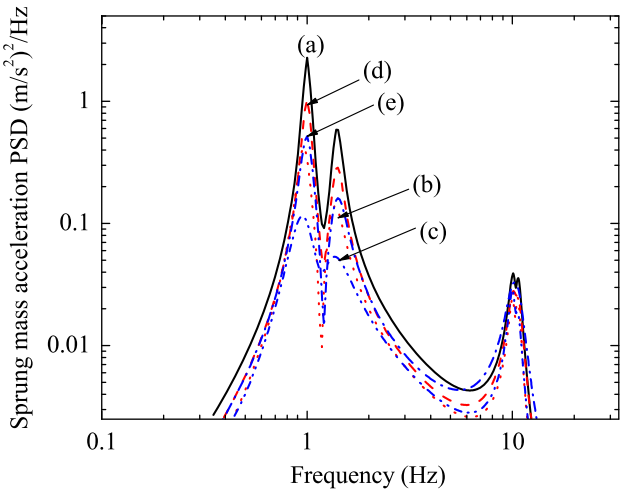

Fig. 18. Sprung mass acceleration psd (legends as in Fig. 9).

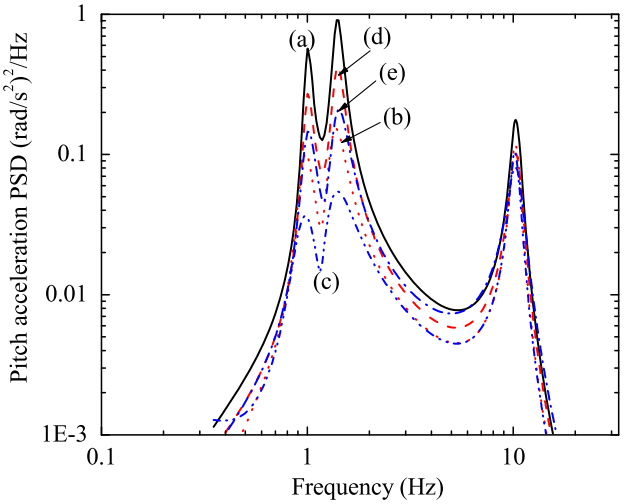

Fig. 19. Pitch acceleration psd (legends as in Fig. 9).

suspension stroke, the performance index with respect to the road holding response is a combination of both the front and rear road holding responses and does not consider them separately. Because of this it may be possible that the rear road holding is not sufficiently weighted in the performance index and hence the performance of the rear road holding is only marginally better than the passive response. The performance is improved with preview information. Results of the equivalent linearization for the MR damper are verified with Monte-Carlo simulation results.

Fig. 18 shows the psd of sprung mass acceleration for different suspension systems (a)–(e). The vehicle model considered for the analysis is a four degrees of freedom vehicle model, so four predominant frequencies are observed in the figure. Since the third and fourth predominant frequencies are very close to each other and the corresponding peaks are also of similar magnitudes they are not as distinguishable. It can be seen that, the sprung mass acceleration characteristics as compared to the passive suspension (a), is improved by the active and semi-active suspension system without and with preview ((b)–(e)) at all the predominant frequencies.

The psd of pitch acceleration response for different suspension systems (a)–(e) is shown in Fig. 19. It shows only three predominant frequencies. One of the predominant frequency due to the unsprung mass is attenuated may be due to the damping. It is observed that all other control schemes (b)–(e) perform better than the passive suspension system (a) at all the frequencies.

9. Conclusions

This paper presents a new approach of controlling the stationary response of a half car vehicle model traversing a rough road with constant velocity with semi-active MR damper suspensions. The MR damper performance is sought to be enhanced to that of the performance of active suspensions with H_∞ control without and with preview. A method to determine the weighting factors in the performance index in H_∞ control using a multi-objective optimization procedure is presented. The multi-objective optimization problem is solved by the NSGA II genetic algorithm in combination with Pareto optimal scheme. The equivalent linearization method is used to get the response of the vehicle with MR damper which is modelled by the modified Bouc–Wen model. Results show that the performance of the MR suspension improves with preview information and better than the performance of the passive suspension. The performance of the MR damper suspension with respect to sprung mass acceleration and pitch acceleration do not measure up to the corresponding performances of active suspension with H_∞ control without and with preview. The suspension stroke and road holding performances especially at the rear are almost as good as the performances of the active suspension with H_∞ control without and with preview. In certain cases the MR damper does not perform as well as the H_∞ control with respect to road holding at the rear suspension.

Appendix A

The system matrices $[F]$, $[G]$, $[D_1]$ and $[D_2]$ represented in Eqs. (20) and (25) are given by

$$[F]=\begin{bmatrix} F_x & D_x \\ 0 & F_d \end{bmatrix},\quad [G]=\begin{bmatrix} G_x \\ 0 \end{bmatrix},\quad [G_x]=\begin{bmatrix} 0 & \frac{1}{M} & 0 & \frac{a}{I} & 0 & \frac{-1}{m_f} & 0 & 0 \\ 0 & \frac{1}{M} & 0 & \frac{-b}{I} & 0 & 0 & 0 & \frac{-1}{m_r} \end{bmatrix}^{\mathrm{T}} \tag{A.1}$$

$$[F_x]=\begin{bmatrix} F_{x1} & F_{x3} \\ F_{x2} & F_{x4} \end{bmatrix},\quad [D_1]=\begin{bmatrix} 0_{N_V\times 1} \\ 1 \\ 0 \end{bmatrix},\quad [D_2]=\begin{bmatrix} 0_{N_V\times 1} \\ 0 \\ 1 \end{bmatrix} \tag{A.2}$$

where N_V is the number of vehicle model state variables. For active suspension system $N_V=8$ and 12 for semi-active MR suspension system. The control matrix $[G_x]=0$ for the passive and semi-active suspension system:

$$[D_x]=\begin{bmatrix} 0 & 0 & 0 & 0 & 0 & \frac{K_{tf}}{m_f} & 0 & 0 \\ 0 & 0 & 0 & 0 & 0 & 0 & 0 & \frac{K_{tr}}{m_r} \end{bmatrix}^{\mathrm{T}},\quad [F_d]=\begin{bmatrix} -\alpha_r V & 0 \\ 0 & -\alpha_r V \end{bmatrix} \tag{A.3}$$

For the active suspension system, the system matrix $[F]$ contains $[F_{x1}]$ and $[F_{x2}]$ terms only and are given by

$$[F_{x1}]=\begin{bmatrix} 0 & 1 & 0 & 0 & 0 & 0 & 0 & 0 \\ \frac{-(K_f+K_r)}{M} & \frac{-(C_f+C_r)}{M} & \frac{-(aK_f-bK_r)}{M} & \frac{-(aC_f-bC_r)}{M} & \frac{K_f}{M} & \frac{C_f}{M} & \frac{K_r}{M} & \frac{C_r}{M} \\ 0 & 0 & 0 & 1 & 0 & 0 & 0 & 0 \\ \frac{-(aK_f-bK_r)}{I} & \frac{-(aC_f-bC_r)}{I} & \frac{-(a^2K_f+b^2K_r)}{I} & \frac{-(a^2C_f+b^2C_r)}{I} & \frac{-aK_f}{I} & \frac{-aC_f}{I} & \frac{-bK_r}{I} & \frac{-bC_r}{I} \end{bmatrix} \tag{A.4}$$

$$[F_{x2}]=\begin{bmatrix} 0 & 0 & 0 & 0 & 0 & 1 & 0 & 0 \\ \frac{K_f}{m_f} & \frac{C_f}{m_f} & a\frac{K_f}{m_f} & a\frac{C_f}{m_f} & \frac{-(K_f+K_{tf})}{m_f} & \frac{-C_f}{m_f} & 0 & 0 \\ 0 & 0 & 0 & 0 & 0 & 0 & 0 & 1 \\ \frac{K_r}{m_r} & \frac{C_r}{m_r} & \frac{-bK_r}{m_r} & \frac{-bC_r}{m_r} & 0 & 0 & \frac{-(Kr+Ktr)}{m_r} & \frac{-C_r}{m_r} \end{bmatrix} \tag{A.5}$$

For the passive (semi-active MR suspension with 0 A) and semi-active suspension system the matrix $[F_{x1}] = [[F_{x11}][F_{x12}]]$, $[F_{x2}]$, $[F_{x3}] = [[F_{x31}][F_{x32}]]$ and $[F_{x4}] = [[F_{x41}][F_{x42}]]$ are, respectively, given by

$$[F_{x11}] = \begin{bmatrix} 0 & 1 & 0 \\ \dfrac{-K_r - K_{2f} - K_{2r} - K_f}{M} & \dfrac{-C_{2f} - C_{2r} + C_{2f}^2 + C_{2r}^2/(C_{1f} + C_{2f})}{M} & \dfrac{b(K_r + K_{2r}) - a(K_f + K_{2f})}{M} \\ 0 & 0 & 0 \\ \dfrac{-a(K_f + K_{2f}) + b(K_r + K_{2r})}{I} & \dfrac{C_{2f}^2 a/(C_{1f} + C_{2f}) - C_{2r}^2 b/(C_{1r} + C_{2r}) + C_{2r} b - C_{2f} a}{I} & \dfrac{-a^2(K_f + K_{2f}) - b^2(K_r + K_{2r})}{I} \\ 0 & 0 & 0 \\ \dfrac{K_f + K_{2f}}{m_f} & \dfrac{(C_{2f} - C_{2f}^2/(C_{1f} + C_{2f}))}{m_f} & \dfrac{a(K_f + K_{2f})}{m_f} \end{bmatrix} \tag{A.6}$$

$$[F_{x12}] = \begin{bmatrix} 0 & 0 & 0 \\ \dfrac{(-C_{2f} a + C_{2r} b - (C_{2f}^2 . b - C_{2f}^2 a)/(C_{1f} + C_{2f}))}{M} & \dfrac{(K_f + K_{2f} + (C_{2f} K_{1f}/(C_{1f} + C_{2f})))}{M} & \dfrac{C_{2f} C_{1f}/(C_{1f} + C_{2f})}{M} \\ 1 & 0 & 0 \\ \dfrac{(C_{2f}^2/(C_{1f} + C_{2f}) - C_{2f}) a^2 + (C_{2r}^2/(C_{1r} + C_{2r}) - C_{2r}) a^2}{I} & \dfrac{a(K_f + K_{2f} + C_{2f} K_{1f}/(C_{1f} + C_{2f}))}{I} & \dfrac{(C_{2f} C_{1f} a/(C_{1f} + C_{2f}))}{I} \\ 0 & 0 & 1 \\ \dfrac{a(C_{2f} - (C_{2f}^2/(C_{1f} + C_{2f})))}{m_f} & \dfrac{(-K_{tf} - K_f - K_{2f} - (C_{2f} K_{1f}/(C_{1f} + C_{2f})))}{m_f} & \dfrac{(-(C_{2f} C_{1f}/(C_{1f} + C_{2f})))}{m_f} \end{bmatrix} \tag{A.7}$$

$$[F_{x2}] = \begin{bmatrix} 0 & 0 & 0 & 0 & 0 & 0 \\ \dfrac{(K_r + K_{2r})}{m_r} & \dfrac{(C_{2r} - (C_{2r}^2/(C_{1r} + C_{2r})))}{m_r} & \dfrac{-b(K_r + K_{2r})}{m_r} & \dfrac{b(-C_{2r} + (C_{2r}^2/(C_{1r} + C_{2r})))}{m_r} & 0 & 0 \\ 0 & \dfrac{C_{2f}}{(C_{1f} + C_{2f})} & 0 & \dfrac{aC_{2f}}{(C_{1f} + C_{2f})} & \dfrac{K_{1f}}{(C_{1f} + C_{2f})} & \dfrac{C_{1f}}{(C_{1f} + C_{2f})} \\ 0 & -\dfrac{C_{hf} C_{2f}}{(C_{1f} + C_{2f})} & 0 & \dfrac{-aC_{hf} C_{2f}}{(C_{1f} + C_{2f})} & -\dfrac{C_{hf} K_{1f}}{(C_{1f} + C_{2f})} & \dfrac{-C_{hf} C_{1f}}{(C_{1f} + C_{2f})} + C_{hf} \\ 0 & \dfrac{C_{2r}}{(C_{1r} + C_{2r})} & 0 & \dfrac{-bC_{2r}}{(C_{1r} + C_{2r})} & 0 & 0 \\ 0 & -\dfrac{C_{hr} C_{2r}}{(C_{1r} + C_{2r})} & 0 & \dfrac{bC_{hr} C_{2r}}{(C_{1r} + C_{2r})} & 0 & 0 \end{bmatrix} \tag{A.8}$$

$$[F_{x31}] = \begin{bmatrix} 0 & 0 & 0 \\ \dfrac{K_r + K_{2r} + (C_{2r} K_{1r}/(C_{1r} + C_{2r}))}{M} & \dfrac{C_{2r} C_{1r}/(C_{1r} + C_{2r})}{M} & \dfrac{-C_{2f} K_{1f}/(C_{1f} + C_{2f})}{M} \\ 0 & 0 & 0 \\ \dfrac{b(-K_r - K_{2r} - C_{2r} K_{1r}/(C_{1r} + C_{2r}))}{I} & \dfrac{-bC_{2r} C_{1r}/(C_{1r} + C_{2r})}{I} & \dfrac{-aC_{2f} K_{1f}/(C_{1f} + C_{2f})}{I} \\ 0 & 0 & 0 \\ 0 & 0 & \dfrac{C_{2f} K_{1f}/(C_{1f} + C_{2f})}{m_f} \end{bmatrix} \tag{A.9}$$

$$[F_{x32}] = \begin{bmatrix} 0 & 0 & 0 \\ \dfrac{-\alpha_{1f} C_{2f}/(C_{1f} + C_{2f})}{M} & \dfrac{-C_{2r} K_{1r}/(C_{1r} + C_{2r})}{M} & \dfrac{-\alpha_{1r} C_{2r}/(C_{1r} + C_{2r})}{M} \\ 0 & 0 & 0 \\ \dfrac{-\alpha_{1f} C_{2f} a/(C_{1f} + C_{2f})}{I} & \dfrac{bC_{2r} K_{1r}/(C_{1r} + C_{2r})}{I} & \dfrac{\alpha_{1r} bC_{2r}/(C_1 + C_2)}{I} \\ 0 & 0 & 0 \\ \dfrac{\alpha_{1f} C_{2f}/(C_{1f} + C_{2f})}{m_f} & 0 & 0 \end{bmatrix} \tag{A.10}$$

$$[F_{x41}] = \begin{bmatrix} 0 & 1 & 0 \\ \dfrac{-K_{tr}-K_r-K_{2r}-(C_{2r}K_{1r}/(C_{1r}+C_{2r}))}{m_r} & \dfrac{-C_{2r}C_{1r}/(C_{1r}+C_{2r})}{m_r} & 0 \\ 0 & 0 & \dfrac{-K_{1f}}{(C_{1f}+C_{2f})} \\ 0 & 0 & \dfrac{C_{hf}K_{1f}}{(C_{1f}+C_{2f})} \\ \dfrac{K_{1r}}{(C_{1r}+C_{2r})} & \dfrac{C_{1r}}{(C_{1r}+C_{2r})} & 0 \\ \dfrac{-C_{hr}K_{1r}}{(C_{1r}+C_{2r})} & \dfrac{-C_{hr}C_{1r}}{(C_{1r}+C_{2r})}+C_{hr} & 0 \end{bmatrix} \tag{A.11}$$

$$[F_{x42}] = \begin{bmatrix} 0 & 0 & 0 \\ 0 & \dfrac{C_{2r}K_{1r}}{m_r(C_{1r}+C_{2r})} & \dfrac{C_{2r}\alpha_{1r}}{m_r(C_{1r}+C_{2r})} \\ \dfrac{-\alpha_{1f}}{(C_{1f}+C_{2f})} & 0 & 0 \\ \dfrac{C_{hf}\alpha_{1f}}{(C_{1f}+C_{2f})}-K_{hf} & 0 & 0 \\ 0 & \dfrac{-K_{1r}}{(C_{1r}+C_{2r})} & \dfrac{-\alpha_{1r}}{(C_{1r}+C_{2r})} \\ 0 & \dfrac{C_{hr}K_{1r}}{(C_{1r}+C_{2r})} & \dfrac{C_{hr}\alpha_{1r}}{(C_{1r}+C_{2r})}-K_{hr} \end{bmatrix} \tag{A.12}$$

The computation of the vehicle response statistics is obtained using zero-lag covariance matrix approach by solving a matrix Lyapunov equation,

$$[F][P]+[P][F]^{\mathrm{T}}+[D_1][Q][D_1]^{\mathrm{T}}+[D_2][Q][D_2]^{\mathrm{T}}+\phi(t,t-t_w)[D_1][Q][D_2]^{\mathrm{T}}+[D_2][Q][D_1]^{\mathrm{T}}(\phi(t,t-t_w))^{\mathrm{T}}=0 \tag{A.13}$$

Appendix B

The matrices $[A]$, $[B]$ and $[N]$ given in Eq. (27) can be represented as $[A]=[C_{yu}]^{\mathrm{T}}[C_{yu}]$, $[B]=[D_{yu}]^{\mathrm{T}}[D_{yu}]$, $[N]=[C_{yu}]^{\mathrm{T}}[D_{yu}]$, where the matrices $[C_{yu}]=[[C_{yu1}][C_{yu2}]]$ and $[D_{yu}]$ are given by

$$[C_{yu1}] = \begin{bmatrix} \dfrac{-\sqrt{\rho_1}(K_f+K_r)}{M} & \dfrac{-\sqrt{\rho}_1(C_f+C_r)}{M} & \dfrac{-\sqrt{\rho_1}(aK_f-bK_r)}{M} & \dfrac{-\sqrt{\rho_1}(aC_f-bC_r)}{M} & \dfrac{\sqrt{\rho_1}K_f}{M} \\ \dfrac{-\sqrt{\rho_2}(aK_f-bK_r)}{I} & \dfrac{-\sqrt{\rho_2}(aC_f-bC_r)}{I} & \dfrac{-\sqrt{\rho_2}(a^2K_f+b^2K_r)}{I} & \dfrac{-\sqrt{\rho_2}(a^2C_f+b^2C_r)}{I} & \dfrac{\sqrt{\rho_2}aK_f}{I} \\ \sqrt{\rho_3} & 0 & a\sqrt{\rho_3} & 0 & -\sqrt{\rho_3} \\ \sqrt{\rho_4} & 0 & -b\sqrt{\rho_4} & 0 & 0 \\ 0 & 0 & 0 & 0 & \sqrt{\rho_5} \\ 0 & 0 & 0 & 0 & 0 \\ 0 & 0 & 0 & 0 & 0 \\ 0 & 0 & 0 & 0 & 0 \end{bmatrix} \tag{B.1}$$

$$[C_{yu2}] = \begin{bmatrix} \dfrac{\sqrt{\rho_1}C_f}{M} & \dfrac{\sqrt{\rho_1}K_r}{M} & \dfrac{\sqrt{\rho_1}C_r}{M} & 0 & 0 \\ \dfrac{\sqrt{\rho_2}aC_f}{I} & \dfrac{-\sqrt{\rho_2}bK_r}{I} & \dfrac{-\sqrt{\rho_2}bC_r}{I} & 0 & 0 \\ 0 & 0 & 0 & 0 & 0 \\ -\sqrt{\rho_4} & 0 & 0 & 0 & 0 \\ 0 & 0 & 0 & -\sqrt{\rho_5} & 0 \\ 0 & \sqrt{\rho_6} & 0 & 0 & -\sqrt{\rho_6} \\ 0 & 0 & 0 & 0 & 0 \\ 0 & 0 & 0 & 0 & 0 \end{bmatrix} \tag{B.2}$$

$$[D_{yu}] = \begin{bmatrix} \frac{\sqrt{\rho_1}}{M} & \frac{\sqrt{\rho_2}a}{I} & 0 & 0 & 0 & 0 & \sqrt{\rho_7} & 0 \\ \frac{\sqrt{\rho_1}}{M} & \frac{-\sqrt{\rho_2}b}{I} & 0 & 0 & 0 & 0 & 0 & \sqrt{\rho_8} \end{bmatrix}^{\mathrm{T}} \tag{B.3}$$

Appendix C

The terms P_1 and P_2 given in Eq. (35) can be represented as $P_1 = P_{1a} + P_{1b}$ and $P_2 = P_{2a} + P_{2b}$ and are given by

$$P_{1a} = \int_0^{t_p} \phi(t, t-\sigma)[G]\{C_b\} \exp([F] - [G]\{C_a\}\sigma)^{\mathrm{T}}[S][D_1]\frac{Q}{2}\mathrm{d}\sigma \tag{C.1}$$

$$P_{1b} = \int_0^{t_p+t_w} \phi(t, t-(\sigma - t_w))[G][C_b] \exp[([F] - [G][C])^{\mathrm{T}}\sigma][S][D_2]\frac{Q}{2}\mathrm{d}\sigma, \quad \sigma \geqslant t_w$$
$$\text{otherwise } P_{1b} = 0, \quad \sigma < t_w \tag{C.2}$$

$$P_{2a} = \int_0^{t_p} \phi(t, t-(\sigma + t_w))[G]\{C_b\} exp([F] - [G]\{C_a\}\sigma)^{\mathrm{T}}[S][D_1]\frac{Q}{2}\mathrm{d}\sigma \tag{C.3}$$

$$P_{2b} = \int_0^{t_p+t_w} \phi(t, t-\sigma)[G][C_b] \exp[([F] - [G][C])^{\mathrm{T}}\sigma][S][D_2]\frac{Q}{2}\mathrm{d}\sigma \tag{C.4}$$

References

[1] D. Karnopp, Active and passive isolation of random vibrations, *Isolation of Mechanical Vibration, Impact and Noise, AMD, ASME Monograph*, Vol. 1 (1), 1973, pp. 64–86.
[2] J.K. Hedrick, Railway vehicle active suspensions, *Vehicle System Dynamics* 10 (1981) 267–283.
[3] R.M. Goodall, W. Kortum, Active controls in ground transportation—a review of the state of the art and future potential, *Vehicle System Dynamics* 12 (1983) 225–257.
[4] G.V. Raju, S. Narayanan, Optimal estimation and control of non-stationary response of a two-degree-of-freedom vehicle model, *Journal of Sound and Vibration* 149 (3) (1991) 413–428.
[5] M.M. Elmadany, Z. Abduljabbar, Linear quadratic gaussian control of a quarter car suspension, *Vehicle System Dynamics* 32 (1999) 479–497.
[6] T. Yoshimura, K. Nakaminami, M. Kurimoto, J. Hino, Active suspension of passenger cars using linear and fuzzy-logic controls, *Control Engineering Practice* 7 (1999) 41–47.
[7] E.K. Bender, Optimum linear preview control with application to vehicle suspension, *Transactions of ASME Journal of Basic Engineering* 90 (1968) 213–221.
[8] S. Senthil, S. Narayanan, Optimal preview control of a two dof vehicle model using stochastic optimal control theory, *Vehicle System Dynamics* 25 (1996) 413–430.
[9] J. Marzbanrad, G. Ahmadi, H. Zohoor, Y. Hojjat, Stochastic optimal preview control of a vehicle suspension, *Journal of Sound and Vibration* 275 (2004) 973–990.
[10] L.V.V. Gopala Rao, S. Narayanan, Preview control of random response of a half-car vehicle model traversing rough road, *Journal of Sound and Vibration* 310 (1–2) (2008) 352–365.
[11] D.C. Karnopp, M.J. Crosby, R.A. Harwood, Vibration control using semi-active force generators, *ASME Journal of Engineering for Industry* 96 (2) (1974) 619–626.
[12] D.L. Margolis, Semi-active heave and pitch control for ground vehicles, *Vehicle System Dynamics* 11 (1982) 31–42.
[13] D.N.L. Horten, LD.A. Crolla, Theoretical analysis of a semi-active suspension fitted to an off-road vehicle, *Vehicle System Dynamics* 15 (1986) 351–372.
[14] G. Verros, S. Natsiavas, G. Stepan, Control and dynamics of quarter-car models with dual-rate damping, *Journal of Vibration and Control* 6 (2000) 1045–1063.
[15] D. Sammier, S. Oliver, L. Dugard, Skyhook and H_∞ control of semi-active suspensions: some practical aspects, *Vehicle System Dynamics* 39 (4) (2003) 279–308.
[16] L.V.V. Gopala Rao, S. Narayanan, Control response of a quarter car vehicle model with optimal sky-hook damper, *International Journal of Vehicle Autonomous System* 6 (3/4) (2008) 396–418.
[17] A. Hac, I. Youn, Optimal semi-active suspension with preview based on a quarter car model, *Transactions of ASME Journal of Vibration and Acoustics* 114 (1992) 84–92.
[18] A. Hac, I. Youn, Optimal design of active and semi-active suspension including time delays and preview, *Transactions of ASME Journal of Vibration and Acoustics* 115 (1993) 498–508.
[19] M. Ahmadian, C.A. Pare, A quarter-car experimental analysis of alternative semiactive control methods, *Journal of Intelligent Material Systems and Structures* 11 (8) (2000) 604–612.
[20] G.Z. Yao, F.F. Yap, G. Chen, W.H. Li, S.H. Yeo, MR damper and its application for semi-active control of vehicle suspension system, *Mechatronics* 12 (2002) 963–973.
[21] W.K. Baek, J.S. Lee, T.H. Kang, S.W. Ryu, Quarter car vibration simulation using an empirical magnetorheological damper model, *Twelfth International Congress on Sound and Vibration*, Lisbon, July 11–14, 2005.
[22] H. Du, K.Y. Sze, J. Lam, Semi-active H_∞ control of vehicle suspension with magneto-rheological dampers, *Journal of Sound and Vibration* 283 (1) (2005) 981–996.
[23] S.B. Choi, S.H. Lee, Y.P. Park, H_∞ control performance of a full vehicle suspension featuring magnetorheological dampers, *Vehicle System Dynamics* 38 (5) (2002) 341–360.
[24] J. Reji, P. Narayana, Magnetorheological fluid composition and a process for preparation thereof, US Patent Number 6875368, 5th April 2005.
[25] K. Deb, *Multi-objective Optimization using Evolutionary Algorithms*, Wiley, West Sussex, England, 2002.
[26] R. Bouc, Forced vibration of mechanical systems with hysteresis, *Proceedings of 4th Conference on Nonlinear Oscillations*, Czechoslovakia, 1967.

[27] T.T. Baber, Y.K. Wen, Random vibration of hysteretic degrading system, *Proceedings of the ASCE Specially Conference on Probabilistic Mechanics and Structural Reliability*, Vol. 21, 1979, pp. 73–88.
[28] W.D. Iwan, I.M. Yang, Application of statistical linearization techniques to nonlinear multi degree of freedom systems, *Transactions of ASME Journal of Applied Mechanics* (1972) 545–550.
[29] Y.K. Wen, Equivalent linearization for hysteretic systems under random excitation, *Transactions of ASME Journal of Applied Mechanics* 47 (1980) 150–154.
[30] J.E. Hurdato, A.H. Barbat, Equivalent linearization of the Bouc–Wen hysteretic model, *Engineering Structures* 24 (2002) 373–383.
[31] R.S. Prabakar, C. Sujatha, S. Narayanan, Magnetorheological damper for vehicular applications: fabrication, experimental and mathematical characterization, *International Conference on Theoretical*, *Applied*, *Computational and Experimental Mechanics* (*ICTACEM 2007*), IIT Kharagpur, India, Paper id 321, December 27–29, 2007.
[32] J.B. Burl, *Linear Optimal Control*, Addition-Wesley, California, 1999.
[33] K. Zhou, J.C. Doyle, *Essentials of Robust Control*, Prentice-Hall, Menlo Park, California.
[34] S. Senthil, Optimal Preview Control Model in Stationary and Nonstationary Response of Road Vehicles, PhD Thesis, Indian Institute of Technology Madras, Chennai, India, 1995.
[35] M. Shinozuka, C.M. Jan, Digital simulation of random process and its applications, *Journal of Sound and Vibration* 25 (1972) 111–128.